Chapter One

Introduction

1.1. Background:

Nanoparticales are particles between 1 and 100 nanometers in size .In nanotechnolog aparticle is defined as a small opject that behaves as awhol unit with respect to its transport and properties.particles are further classified according to diameter [1] Uitrafine particles are the same as nanoparticles and between 1 and 100 nanometer in size fin particles are sized between 100 and 2500 and 10000 nanometers. .Nanoparticle research is currently an area of intense scientific interest due to a wide variety of potential applications in biomedical optical and electronic fields.[2][3][4][5] Although in general nanoparticles are considered a discovery of modern science they actually have a long history .nanoparticles were used by artisans as far back as the ninth century in Mesopotamia for generating a glittering effect on the surface of pots. [6][7]

Even these days pottery from the Middle Ages and Renaissance often retain a distinct gold or copper colored metallic glitter.This Luster is caused by a metallic film that a plied to the transparent surface of a glazing. The Luster can still be visible if the film has resisted atmospheric oxidation and other weathering.[6][7]

Luster technique showed that ancient craftsmen had a rather sophisticated empirical Knowledge of materials. The technique originated in the Muslim World .As Muslims were not allowed to use gold in artistic representations they sought a way to create a similar effect without using real gold. The solution they found was using Luster[7].Michael Faraday Provided the first description in scientific terms of the optical properties of nanometer-scale metals in his classic 1857paper .In a subsequent paper the author (Turner) points out that:"it is well know that when thin leaves of gold or silver are mounted upon glass and heated to a temperature that is well below a red head (~500C)a remarkable change of properties takes place whereby the continuity of the metallic film is destroyed. Th result is that white light is now freely transmitted reflection is correspondingly diminished while the electrical resistivity is enormously increased".[8][9][10]

1.2. Properties of copper oxide nano particles:

Nanoparticles are of great scientific interest as they are in fact a bridge between bulk materials and atomic or molecular strctures.Abulk material should have constant physical properties regardless of its size but at the nanoscale size-dependent properties are often observed. Thus the properties of materials change as size approaches the nanoscale and as the percentage of atoms at the surface of a material becomes significant.for bulk marterials larger than one micrometer (or micron) the percetage of atoms at the surface is in insignificant in relation to the number atoms in the bulk of the material. Nanoparticles often possess unexpected optical properties as they are small enough to confine their electrons and produce quantum effects[4]. for example gold nanoparticles appear deep-red to black in solution. Nanoparticles of yellow gold and grey silicon are red in color. Gold nanoparticles melt at much lower temperatures (~300C for 2.5nm size) than the gold slabs (1064C).[11] Absorption of solar radiation is much higher in materials composed of nanoparticles than it is in thin films of continuous sheets of material. In both solar PV and solar thermal applications controlling the size shape and material of the particles it is possible to control solar a bsorption.[3][5][12] Other size –dependent property changes include quantum confinement in semiconductor particles surface plasmon resonance [4] . in some metal particles and superparamagnetism in magnetic materials. What would appear ironic is that the changes in physical properties are not always desirable. Ferromagnetic materials smaller than 10 nm can switch their magnetisation direction using room temperature thermal energy thus making them unsuitable for memory storage.[13] Suspensions of nanoparticles are possible since the interaction of the partical surface with the solvent is strong enough to overcome density differences which otherwise uaually result in amaterial either sinking or floating in a liquid.

The high surface area to volume ratio of nanoparticles provides a tremendous driving force for diffusion especially at elevated temperatures. Sintering can take place at lower temperatures over shorter time scales than for larger particles. In theory this does not affect the density of the final product though difficulties and the tendency of nanoparticles to a gglomerate complicates matters. Moreover nanoparticles have been

found to impart some extra properties to Uarious day to day products. For example the presence of titanium dioxide nanoparticles imparts wat we call the self-cleaning effect and the size being nanorange the particles cannot be observed. Zin oxide particles have been found to have superior UV blocking properties compared to its bulk substitute. This is one of the reasons why it is often used in the preparation of sunscreen Iotions [14] is completely photostable[15] and toxic.[16][17][18][19][20][21]

Copper oxide (CuO) nanoparticles are synthesized by aqueous precipitation method using copper chloride as a precursor and NaOH as stabilizing agent. This gives large scale production of nanoparticles. In the last decade, the developments of nano size materials of metal and metal oxide particles are intensively pursued because of their prominence in different fields of applications. In all the transition metal oxides, CuO nanoparticles are used for the applications of magnetic storage devices, solar energy transfer, sensors and super capacitors, Chemical plants etc. In general there are number of metal oxides are available in nature but some of the metal oxides are most useful in accordance with their applications in day to day life in science and technology. In the periodic table transition metals are large in number and have number of applications in differentfields. Among the oxides of transition metals, copper oxide nanoparticles are of special interest because of their efficiency as nanofluid in heat transfer application. For example it has been reported that addition of CuO improves the thermal conductivity of water [22, 23].CuO is a semiconducting compound with a narrow band gap and used for photoconductive and Photo thermal applications. Some transition metal oxides like ZnO, TiO_2 and Fe_3O_4 etc. proved as potential candidates for so many applications. In the same way CuO is also one of the useful metal oxides and which has so many applications in various fields. The uniqueness of CuO nanoparticles is even though, they are metallic in bulk but they behave like semiconductors when they are in nano size. Semiconducting materials have been particularly interesting because of their great practical importance in electronic and optoelectronic devices, such as electrochemical cell, gas sensors, magnetic storage devices, field emitters, high-tc super conductors, nanofluid and catalysts etc. Due to the potentiality of CuO, it acts as a catalyst; whereas all metal oxides are not useful for the catalytic activity. In the fabrication of super capacitors also CuO is very useful and in nano range it has the wide band gap nearly equal to ZnO. The favourable band gap of CuO around 2.6 eV makes it useful for solar energy conversion and it can be used as solar cell window material.

CuO nanoparticles act as a good catalyst in some of the chemical reactions. CuO nanoparticles were prepared by sol-gel method. In this method $CuCl_2.2H_2O$. (0.2 M) is added with acetic acid and heated to 100 0C with continuous stirring. To control the pH of the above solution, NaOH is added to the solution till pH reached desired value. The color of the solution changed from sky blue to black with precipitation. The black precipitation was washed 3 -4 times with distilled water. Finally the solution was centrifuged and dried in air for one day. The CuO nanoparticles were characterized by studying their structure with X-ray diffraction and composition by energy dispersive X-ray analysis. The size of the nanoparticles is estimated by XRD and transmission electron microscopy. These nanoparticles are used to prepare Nano fluid with base fluid as deionized water and experiment is conducted to determine critical heat flux at different weight percent concentration in which maximum enhancement in CHF at 1.5 weight percent of CuO Nano fluid (57.26%).

1.3 Preparation of CuO nano particle:

Nanoparticles are prepared by using economical Sol-Gel method and characterization is done to finalize the size and purity of prepared nanoparticles.

1.3.1. Sol-gel method of synthesis:

There are various techniques to prepare nanocrystals e.g. sputtering, laser ablation, cluster deposition, sol-gel method etc. The synthesis of CuO is preferred by sol-gel route because this method is easy and economical [24, 25].The sol-gel process involves the formation of colloidal suspension (sol) and gelatin of the sol to form a network in continuous liquid phase (gel).The precursors for synthesizing these colloids consist usually of a metal or metalloid element surrounded by various reactive legends. The aqueous solution of $CuCl_2.2H_2O$ (0.2 M) is prepared in cleaned round bottom flask. 1 ml of glacial acetic acid is added to above aqueous solution and heated to 100 °C with constant stirring. 8 M NaOH is added to above heated solution till pH reaches to 7. The color of the solution turned from green to black immediately and the large amount of black precipitate is formed immediately.

.The precipitate is centrifuged and washed 3 -4 times with deionized water. The obtained precipitate was dried in air for 24 hours. This powder is further used for the characterization of CuO nanoparticles. The chemical reaction is as follows,

$$CuCl_2 + 2\ NaOH \rightarrow Cu\ (OH)_2 + 2\ NaCl \rightarrow (1.1)$$
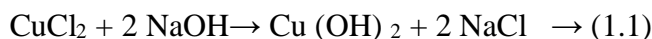
And copper hydroxide decomposes into copper oxide on heating as follows,

$$Cu(OH)_2 \rightarrow CuO + H_2O \rightarrow (1.2)$$

1.4. Understanding silica-supported metal catalysts Pd/silica as a case study:

The study of metal particles on oxide supports is of importance in heterogeneous catalysis because the size and nature of the interaction of a metal particle with an oxide support are critical in determining catalytic activity and selectivity. [1–3] It is well-known that metals on reducible oxides such as TiO_2. [4, 5] Exhibit a strong metal–support interaction (SMSI). On the other hand, irreducible oxides like SiO_2 are assumed to be relatively inert. However, in certain cases, silica has been shown to exhibit a metal–support interaction following high temperature treatment [6-8] Oxidation and reduction at elevated temperatures are essential steps for the preparation of supported, high surface area catalysts; however, these treatments can cause morphological changes of the dispersed metal particles arising from sintering and/or metal– support interactions. Therefore, it is of considerable importance to investigate and define optimal conditions for catalyst preparation, pretreatment and activation. [9] Depending on the particular metal–oxide system, various morphological changes resulting from a metal–support interaction have been reported, namely sintering [10-14], Encapsulation [15, 16], Inter-diffusion. [17–27] And alloy formation. [28, 29] In particular, silicide formation from metals supported on silica has received considerable attention because of the importance of the metal–silica interface to numerous technologies. For example, studies of metal–oxide–semiconductor (MOS) structures are directly related to many aspects of semiconductor technology including the design of MOS devices. In addition, metallization is important for creating contact layers and durable electrically conducting vias on insulating substrates for semiconductor devices [30, 31.] Furthermore, silicide formation between metals and SiO_2 in a catalyst has been shown to alter catalytic activity and selectivity. [32, 33] For instance, it has been shown that Pd-silicide, formed during the high

temperature reduction of Pd/SiO$_2$, dramatically increases selectivity for the isomerization of neopentane.[33]

However, in spite of the numerous studies on metals supported on SiO$_2$ at elevated temperatures, there are still controversial and unresolved issues regarding the nature of the metal–support interaction in silica-supported catalysts, namely:

1- The nature of the metal–support interaction between metals and SiO$_2$;

2- The morphological changes that occur during the high temperature reduction of metals supported on SiO$_2$;

3- The role of oxygen vacancies in the inter-diffusion of metals into SiO$_2$;

4- The extent to which silicide's are formed by the direct interaction between metals and SiO2;

5- The role of the silicon substrate, frequently used to prepare SiO2 thin films, in metal silicide formation;

6- The composition, if formed, of metal silicide's;

7- The mechanism of silicide formation between metals and SiO$_2$.

1.5. Chemical Properties:

The chemical properties of copper oxide nanoparticles are outlined in the following table:

Table 1.1 Chemical properties

Chemical symbol	CuO
Group	Copper 4 Oxygen 16
Electronic Configuration	Copper[Ar]3d^{10}4S^{1} Oxygen[He]2S^{2}2P^{4}

1.6. Physical Properties:

Table 1.2 physical properti

Density	6.31 g\cm^3
Molar mass	79.55 g\mol

1.7. Thermal Properties:

Table 1.3 Thermal properties of copper oxide nanoparticales:

Melting point	1201 C^0
Boiling point	2000 C^0

1.8Applications:

The key applications of copper oxide nanoparticles are as follows:

1. As burning rate catalyst in rocket propellant. It can greatly improve the homogeneous propellant burning rate, lower pressure index, and also perform better as a catalyst for the AP composite propellant.

2. Can be applied to the catalyst, superconducting materials, thermoelectric materials, sensing materials, glass, ceramics and other fields.

3. As ceramic resistors, magnetic storage media, gas sensors, near-infrared tilters, photoconductive and photo thermal applications.

4. as semiconductors, solar energy transformation, and high-tech superconductors.

1.9 Experimental of understanding silica-supported metal catalyst:

Details of the ultrahigh vacuum chamber, equipped with scanning tunneling microscope (STM), X-ray photoelectron spectroscopy (XPS), low energy electron diffraction (LEED), and Auger electron spectroscopy (AES) with a base pressure of 5×10^{-10} mbar, have been published. [34] Briefly, this apparatus is equipped with a double-pass cylindrical mirror analyzer, reverse view LEED optics, and a room temperature STM (Omicron). Typically, the STM images were acquired in the constant current mode with a ~2 V tip bias and a tunneling current of ~0.1 nA. Ultrahigh purity (99.999%) oxygen from MG industries was used. A Mo (1 1 2) crystal, oriented with an accuracy of <0.25 ∘ (from Mate), was cleaned by flashing to 2100 K until no evidence of carbon and oxygen was detectable by AES. A W–5% Re/W–26% Re thermocouple was used to calibrate an optical pyrometer (OMEGA OS3700) that was then employed to monitor the crystal temperature during the STM experiments.

1.9.1 High surface area, silica-supported metal catalysts:

Reduction at elevated temperature is one of the important steps in the synthesis of supported metal catalysts; however, heating a supported metal catalyst can cause morphological changes in the metal particles depending upon the particular metal–oxide system. Chang et al. [9] have shown that various metal–support interactions are operative for Pd catalysts on various supports, e.g. SiO_2, $Al2O_3$, and TiO_2, using a combination of temperature-programmed reduction and adsorption methods. Hydrogen adsorption experiments by this group on a SiO_2-supported Pd catalyst (1% Pd/SiO_2) showed no significant SMSI interaction even after heating to temperatures as (873K). These results differ markedly from the data obtained for Pd/TiO where a significant reduction of adsorbed hydrogen was attributed to a strong metal–support interaction. The SMSI was attributed to arise via the diffusion of partially reduced $TiO2$ onto the surface of the Pd clusters. Based on these studies, the authors suggested that the tendency for SMSI to occur between dispersed Pd and a support increases in the order: $Pd/SiO_2 < Pd/Al_2O_3 < Pd/TiO_2$. In addition. It was also suggested that Pd/SiO_2 displayed the least tendency to sinter compared with other metal–oxide pairs under identical reduction conditions.

Negligible sintering of Pd/SiO_2 (0.5–25.0% Pd) was reported by Moss et al. [35], who measured the Pd surface area by chemisorption of CO and H2 following two reduction temperatures, 573 and 723 K. Electron micrographs of the Pd/SiO_2 catalysts corresponding to each reduction

temperatures confirmed that no change has occurred in the metal morphology or dispersion; however, the specific catalytic activity for benzene hydrogenation dramatically decreased with an increase in the reduction temperature to 823 K. Three explanations for this were proposed:

(i) a variation in the surface structure of the support.

(ii) Promoters or inhibitors on the Pd or the support, and

(iii) An interaction between the Pd clusters and the support. The latter explanation was based on an X-ray diffraction investigation that indicated formation of a Pd–silicon intermetallic compound.

Direct evidence of Pd-silicide formation due to high temperature reduction has been suggested by Shen et al [32, 33].Their XRD data of a mechanical mixture of Pd powder and silica gel after high temperature reduction (873 K) showed the presence of a Pd3Si species. These authors suggested that the formation of this Pd-silicide species is responsible for the dramatic increase in the selectivity of this catalyst for the isomerization of neopentane. The silicide formation is believed to occur during high temperature reduction by diffusion of Pd atoms into the bulk via oxygen vacancies in the SiO_2. Pure Pd, however, was easily regenerated by the oxidation of the silicide at low temperature. A change in catalytic activity following high temperature reduction has also been observed for Ni/SiO_2 and Pt/SiO_2. Martin et al. [36–39] have shown that the catalytic activity of Ni/SiO_2 (24% of Ni) for ethane hydrogen lysis and benzene hydrogenation decreases by an order of magnitude with an increase in the reduction temperature from 920 to 1120 K. Based on hydrogen chemisorption it was anticipated that reduction at high temperature would lead to sintering of the nickel particles, however, the effects were much larger than that expected from a simple increase in particle size. A similar but more significant effect of high temperature reduction was also observed for a Pt/SiO_2 catalyst.

1.9.2 Model silica-supported metal catalysts:

1.9.2.1. Sintering:

Sintering [40–43] can be understood using the Gibbs–Thompson relationship where larger particles with lower chemical potential will grow at the expense of smaller particles with higher chemical potential, the driving force being the reduction of the total surface energy of the system. Sintering is certainly affected by the environment and can be accelerated by a reactant gas and by temperature. In addition, sintering is strongly dependent on the nature of the metal–support interaction, i.e., the relative strengths of the metal–metal versus the metal–support bond energies. Generally, it is believed that for metals on an irreducible oxide support, the strength of the metal–metal bond is significantly larger than the metal–support bond, leading to a relatively weak metal–support interaction and facile thermal sintering. Pretorius et al [10] .have investigated the interaction between various metals including noble metals and SiO_2 thin films at high temperature (1073 K) using Rutherford backscattering (RBS) and scanning electron microscopy (SEM). Their results show that metals do not react with a SiO_2 substrate whereas Ti,Zr, Hf, V, and Nb do react to form metal silicide's. SEM images also have confirmed that islands of metals tend to coalesce with a high temperature anneal. For noble metals, heats of formation were calculated and found to be positive using the following reaction:

$$M + SiO_2 \rightarrow MSix + MOy. \rightarrow (1.3)$$

It was also suggested that these heats of formation should correlate with the mean electronegativity of the metal, allowing the relative reactivity of a metal with SiO2 to be predicted. With these considerations, metals with an electronegativity of less than 1.5 on the Pauling scale should react with a SiO_2 substrate; the values for noble metals fall within the range 1.67–1.80, and therefore these metals should be unreactive [10].Chen and Schmidt [11].have investigated the effects of reactive gases and temperature on the sintering rates and morphology of Pt particles on amorphous SiO_2. Using transmission electron microscopy the average crystallite size of the Pt particles increased dramatically when heated to 973 K. The structure and chemical properties of model silica-supported metal catalysts have been investigated in our

laboratory using various surface science techniques. [12–14, 44–46]SiO2 thin films were prepared by high temperature co-deposition of Si and oxygen onto a Mo (1 1 0) or Mo (1 0 0) substrate followed by an anneal, a procedure that yields an amorphous oxide film. Temperature-programmed desorption (TPD) experiments for the Cu/SiO2 system showed that the saturation coverage of CO decreases by a factor of 2 with an increase in the annealing temperature from 100 to 900 K. In addition, marked changes in infrared reflection adsorption spectra (IRAS) were also observed. Cu as a function of the pre-anneal temperature. On the as-deposited (100 K) Cu clusters, CO exhibits an IR absorption band centered at 2099 cm^{-1} with a small shoulder on the low-frequency side of the peak. Upon annealing to 300–500 K the 2099 cm^{-1} IRAS of CO on silica-supported Cu as a function of the pre-annealing temperature. Cu was deposited at 100 K and annealed to the indicated temperatures, followed by CO adsorption to saturation at 90 K. TPD from Cu/SiO$_2$/Mo (1 1 0). The silica film is ~10 nm thick and the Cu coverage is ~8 × 1014 atoms/cm2 (~0.6 MLE). The silica film was annealed to 1500 K before Cu deposition. Cu was deposited at 90K and the heating rate for TPD was 10K/s.

Band shifts to 2097 cm^{-1}, and a new band appears at 2070 cm^{-1}. Further heating to 700–900 K results in a splitting of the 2097 cm^{-1} feature into two peaks at 2018 and 2094 cm^{-1}. These CO absorption bands are attributed to several distinct atop CO adsorption sites implying CO adsorption onto various Cu crystalline facets. TPD for CO adsorption at 90 K on Cu/SiO2 annealed to 1200 K shows no evidence for CO adsorption even though Cu is still evident on the surface as evidenced by the Cu TPD. The –peak at 1000 K was assigned to metallic Cu; the –peak (1300 K) was attributed to a Cu species strongly bonded to the SiO2 surface since it's desorption temperature was 200 K higher than the bulk Cu sublimation temperature. In addition, no adsorption of CO on Cu/SiO2, pre-annealed to 1200 K, indicated that this high temperature Cu species is not metallic in nature. The surface structure of supported Pd clusters on similarly prepared silica films was also investigated with IRAS of adsorbed CO., for the as-deposited Pd film, two broad bands were observed at 2110 and 1990 cm^{-1} , corresponding to CO adsorption on atop and bridging sites, respectively. Annealing the films to >500 K leads to a new band at 1890 cm^{-1} , that corresponds to CO adsorbed on threefold hollow sites [14]. In addition, the peak for the atop and bridging bands becomes much sharper for the annealed films.

This narrowing of the peaks is attributed to the formation of stable, extended facets. Shows the oxygen TPD from O/Pd/SiO$_2$ IRAS of CO on a model silica-supported Pd catalyst (θPd = 15 MLE) as a function of pre-annealing temperature. The spectra were collected at 100 K and in 10 −6 Torr CO background. The surface was annealed to 100, 300, 500, 700 and 900 K, respectively.

Oxygen desorption occurs primarily within the temperature range 700–900 K, similar to oxygen desorption from Pd single crystals and foils. In addition, a small oxygen desorption peak is observed between 1200 and 1300 K, the temperature range within which Pd is known to sublime. This high temperature oxygen TPD from O/Pd/SiO$_2$/Mo (1 1 0). The Pd coverage is 6×1015 atoms/cm^2. Oxygen was adsorbed at 100 K to saturation. Desorption feature is attributed to oxygen absorbed within the bulk of the Pd clusters. However, oxygen desorption via decomposition of the silica film at high temperature catalyzed by Pd is also a possibility.

1.9.2.2 Encapsulation:

One deactivation mechanism for supported metal catalysts is encapsulation [1, 15]. Resulting in a reduction in the active metal surface area. This decrease in the ratio of the metal surface area to the metal interface area occurs when hemispherical metal clusters on an oxide surface are partially encapsulated by the oxide support. Powell and Whittington [15].first proposed encapsulation to account for the change in morphology of silica-supported platinum model catalysts following a high temperature anneal. These authors, using SEM, showed that Pt particles became partially immersed in the SiO2 surface with concomitant formation of a SiO2 ridge around the base of the Pt particles when annealed at 1200 and 1375 K. Recently, Van den Outlearn et al. [16,28]. Have investigated the metal–support interaction between Cu and SiO2 using LEIS, AFM, and RBS by preparing very thick SiO2 films (400–500 nm) on a silicon wafer. The LEIS measurements showed that the coverage of Cu gradually decreased following an anneal to 773 K and completely disappeared after an anneal to 923 K indicating that no bare Cu remained on the surface. The RBS data, however, were unchanged following an anneal to 923 K, consistent with encapsulation of the Cu clusters.

1.9.2.3 Inter-diffusion:

Numerous investigations have shown that metals can diffuse into a SiO_2 support. Scott and Lau [17] have investigated the effects of interfacial SiO_2 on th formation of a metal silicide with a silicon substrate using RBS and 16O (d,) 14N/18O (d,) 15N nuclear reactions. A SiO_2 layer was synthesized on a silicon wafer oxidation, then a noble metal, e.g. Pd, Pt, Ni, evaporated onto it. A feature corresponding to a metal silicide was observed at the interfacial region of SiO2 after an anneal to 673–1023 K. As a plausible explanation, the authors suggested the following. Initially, the SiO2 is present as a layer between the metal and the silicon. Upon annealing at a sufficiently high temperature, the metal diffuses through the SiO2 layer to form a silicide. The formation of the silicide gives rise to lateral non-uniformities in the layer such that the barrier to silicon diffusion is significantly lowered, i.e., silicon diffusion, no longer blocked by the SiO2 layer, is facilitated. Schweich et al. Have also investigated Pd-silicide formation on oxidized Si (1 1 1) using XPS and HREELS. These authors showed that a loss feature related to a C–O vibration near 240 mV disappeared after annealing to >510 K implying the disappearance of Pd on SiO2. Furthermore, subsequent to an 820 K anneal, the HREELS spectrum showed a feature similar to that acquired from a freshly prepared SiO2 surface. In addition, XPS spectra showed an additional feature after a 600 K anneal near 336.9 eV in addition to the feature related to Pd0. This additional feature was consistent with the formation of Pd-silicide; silicide formation was confirmed by XPS spectra following an anneal of Pd on a clean Si (1 1 1)-7 × 7 surface. Dall porta et al. [26, 27] have studied the thermal stability of SiO2 films on Si (1 0 0) induced by various metals during a vacuum anneal using scanning Auger microscopy (SAM) and SEM. These authors observed metal-induce decomposition of the SiO2 films and proposed two possible mechanisms, each with a varying dependence on the electronic properties of the metal. One metal type corresponding to s-type, p-type, and transition metals with few d electrons, react directly with SiO2 and lead to homogeneous decomposition. Metals, on the other hand, must diffuse to the interface likely via defects where heterogeneous decomposition occurs. Furthermore, the authors suggest that decomposition of SiO2 by a noble metal is generally exothermic. This excess energy then assists the further reaction of SiO2 and Si to SiO, thereby

enhancing the defect concentration. Alternatively, the altered electronic structure of the metal subsequent to reaction could facilitate the breaking of the Si–O bond.

1.9.2.4. Alloy formation:

Recent study, has shown metal silicide to form between a metal and silica grown on a silicon wafer. In general, it is believed that oxygen vacancies are the primary diffusion pathways for the formation of silicide at the interface between SiO2 and Si. However, studies have shown that metal silicide formation can occur via direct interaction between SiO2 and the metal. As discussed above [16,28], temperature dependent AES studies of Cu supported on thick films of SiO2 (400–500 nm, in order to avoid any influence of underlying Si) clearly show splitting of the Si LVV peak at 92 eV into two peaks at 90 and 94 eV, respectively, due to Cu-silicide formation. Furthermore, this silicide feature in the AES was enhanced with an anneal at 893 K. Very recently, the thermal stability of Pd supported on single crystalline SiO2 thin films grown on Mo (1 1 2) substrate has been investigated in our laboratory using STM and AES techniques. In this work, a Mo substrate rather than a Si substrate was used to support a SiO2 thin film to avoid complications of silicide formation at the Si–SiO2 interface.

Well-ordered, epitaxial SiO2 ultrathin films (~0.4 nm) have been prepared on a Mo (1 1 2) surface in two different ways: (a) vapor deposition of Si onto a Mo (1 1 2) single crystal followed by oxidation and high temperature annealing [47] and (b) vapor deposition of Si onto a (2 × 3)-O oxygen reconstructed Mo (1 1 2) surface followed by oxidation and annealing. [48,49] A typical STM image of SiO2 ultrathin films prepared by the above methods, showing wide terraces and steps consistent with the underlying Mo (1 1 2) substrate. Also, both films show a sharp hexagonal LEED pattern confirming the long-range order of the film; STS as well as MIES and UPS data [50] indicate a wide band gap (~9 eV) and confirm the bulk-like electronic character of the SiO2 surface.

However, STM images of film I show a more defective and less uniform surface compared with film.
The STM images show the nucleation and growth behavior of Pd clusters (~2 monolayer equivalents (MLE)) on these two different SiO2 thin films (I and II) at room temperature.

Show elongated, hemispherical particles at high density and with diameter of 2–3 nm distributed homogeneously on the surface. In larger Pd clusters (3–6 nm), distributed less densely, and are evident. It is generally believed that metal particles nucleate and grow preferentially on point defects on oxide surfaces, presumably at oxygen vacancies [51]. Therefore, the higher number density of the Pd clusters in film me than that of film II suggests a more highly defective surface.

The STM images acquired after annealing to 700 K show no appreciable change with respect to cluster size or shape for either film I or II. However, those images acquired after annealing to 1000 K. The Pd clusters on the more defective SiO2 surface (film I), rather than being 3D, have spread on the SiO2 surface. The Pd clusters on the less defective SiO2 surface (film II) exhibit an elongated rectangular shape with increasing size, a decrease in the number density, and a decrease in the cluster height. The total volume of Pd particles calculated from STM images shows a ∼20% decrease.

This decrease is not due to desorption of Pd since desorption of Pd takes place above 1050 K. It is also quite clear that under our experimental conditions Pd particles on both SiO2 films remain morphologically unperturbed until 700 K, however, clusters on film II sinter between 750 and 1000 K; this sintering is accompanied by inter-diffusion. On the other hand, the behavior observed on film I shows a dramatic change in morphology.

Will be designated "activated", and the specifics of this surface will be addressed subsequently. In order to investigate the thermal stability of the Pd/SiO2 system, annealing was carried out in a step-wise manner. Shows changes in the relative AES intensity ratios of IPd/IMo (a) and IO/IMo (b) during these annealing experiments. Consistent with the STM results, no changes in IPd/IMo or IO/IMo are observed at temperatures to 700 K. However, between 750 and 1050 K, the ratios IPd/IMo decrease while the ratios IO/IMo remain unchanged. Above 1050 K, a marked decrease in IO/IMo occurs and is accompanied by a decrease in IPd and ISi. From previous work in our laboratories, desorption of Pd was shown to begin at ∼1050 K whereas the onset of the decomposition of the SiO2 thin films occurs at ∼1200 K.

Therefore, the concomitant loss of oxygen and silicon above 1050 K due to Pd-induced decomposition of the SiO_2 thin film, either involving the formation of a volatile Pd-silicide or SiO/Si, concurrent with Pd desorption since no characteristic feature of silicide (splitting of the Si LVV peak at 92 eV into two peaks at 90 and 94 eV) was detected by AES.

As mentioned earlier, in Pd/SiO2 high surface area catalysts, evidence for Pd3Si formation has been reported using XRD subsequent to hydrogen reduction at 873 K [33]. In addition, it has also been suggested that point defects on SiO2 thin films are the primary mechanism for inter-diffusion of Pd. In order to investigate the role of point defects, a defective surface was prepared by electron beam bombardment. An electron beam produced a new feature at 92 eV, whose intensity grows with exposure time. This feature is assigned to a Si0 species arising from SiO2 + e-beam   STM images of: (a) a clean SiO2 thin film (200 nm × 200 nm) with a thickness of ~0.4 nm (considered to be the more defective surface); (b) ~2 MLE Pd on SiO2 thin film (a) (100 nm × 100 nm) at room temperature; (c) activated Pd surface (100 nm × 100 nm) taken after a 1000 K anneal of (b); (d) a clean SiO2 thin film (200 nm × 200 nm) with the thickness of ~0.4 nm (considered to be the less defective surface); (e) ~2 MLE Pd on SiO2 thin film (c) (100 nm × 100 nm) at room temperature and (f) Pd surface (100 nm × 100 nm)taken after a 1000 K anneal of (e).

SiO + O2 (g) reaction. However, step-wise annealing, subsequent to the deposition of Pd and annealing below 1000 K followed by deposition of elemental Si, showed no evidence of Pd-silicide, even though Si/Pd and Pd/Si are known to mix readily at this temperature [52–55]. This suggests that Si and Pd nucleate separately on the SiO_2 surface. It is also noteworthy that the deposition of elemental Si on Pd on less defective SiO_2 thin film does not produce a silicide feature. However, point defects, created by electron beam bombardment on an "activated" Pd/SiO_2 surface lead to silicide formation upon annealing to 1000 K (AES spectrum. According to the detailed AES study of Tanaka et al. [56], this silicide is Pd-rich. Alternatively, The plots of AES intensity ratio as a function of annealing temperature: (a) IPd/IMo and (b) IO/IMo. Deposition of 0.5 MLE of Si onto an activated Pd/SiO_2 surface, a silicon-rich silicide was observed after annealing to 1000 K. An even greater silicon-rich silicide was observed following the deposition of 1.0 MLE Si and an anneal to 1000 K. In other words, the composition of the silicide depends on the amount of pre-adsorbed silicon. It is noteworthy that significant loss of

oxygen is evident during silicide formation due to the decomposition of SiO_2. . High resolution AES spectra around Si LVV peak (55–110 eV) region. The splitting of the Si LVV peak at 92 eV into two peaks at 90 and 94 eV indicates silicide feature. (a) Silicide formation induced by point defects from electron beam bombardment and (b) silicide formation induced by (1) 0.5 MLE pre-deposited Si and (2) 1.0 MLE pre-deposited Si. Based on these observations, the following conclusions can be drawn: (a) an "activated" surface is essential for low temperature silicide formation and (b) deposited Si or point defects created by electron beam bombardment aid in the production of silicide at temperatures between 850 and 1000 K as detected by AES. It is also noteworthy that it is possible to reversibly re-oxidize the silicide-containing surface by treatment in 1×10^{-5} mbar of oxygen for 1 h at room temperature. In order to understand the role of Si in the formation of Pd-silicide, step-wise annealing experiments were carried out after depositing a trace of silicon on an "activated" Pd/SiO_2 surface. The amount of silicide increases with the anneal time and is accompanied by loss of oxygen.   .

Silicide formation also induces an increase in the AES intensity ratio of IPd/IMo, consistent with 2D silicide formation on the oxide and segregation of the volatile Pd-silicide to the surface. Based on these results the amount of silicide formed does not depend on the amount of Si deposited, but rather on the annealing time. In other words, a trace of Si acts as an initiator for this reaction. An excess of Si accelerates the reaction and alters the composition of the silicide product.

The nature of the "activated" surface has been studied by STM. High resolution AES spectra near the Si LVV region as a function of annealing time at 1000 K where spectrum 1, 2 and 3 correspond to 2, 12 and 32 min, respectively. (b) A plot of AES intensity ratio as a function of annealing time at 1000 K: (1) IO/IMo and (2) IPd/IMo.

STM images (34 nm × 34 nm) in 3D-view of Pd/SiO2 surfaces acquired after annealing at (a) 300, (b) 800 and (c) 950 K, respectively.

Plot (d) shows change in the average height of the clusters as a function of the annealing temperature.

Pd/SiO$_2$ surface following anneals at 300, 800, and 950 K, respectively. As discussed earlier, no changes in the cluster shape and size are apparent until approximately 700 K. However, it is clear from the images of that the number density of the Pd clusters decreases while the diameter of the Pd clusters increases with an increase in the annealing temperature above 750 K. Shows how the average height of the clusters (calculated from the corresponding STM image) changes with respect to the annealing temperature. These results imply that Pd sintering and inter-diffusion occur simultaneously with an increase in the anneal temperature as shown schematically in. Simple thermodynamic considerations preclude the reaction pathway:

$$Pd + Si_yO_2 \rightarrow PdSi_y + O_2 \text{ (g)}. \rightarrow (1.4)$$

However, for the Cu/SiO$_2$ system, Van den Outlearn Schematic diagram of proposed model for Pd-silicideformation.

Have suggested that the formation of a Cuδ+ species, due to the interaction between the Cu and the support, could alter the surface/interface free energies such that reaction between the SiO$_2$ support and Cu at high temperature can occur. In the present system only the "activated" surface forms silicide via reaction with surface defects (e-beam-induced as well as via deposition of Si) prior to desorption as metallic Pd. Therefore, by analogy to the Cu/SiO$_2$ system, it is likely that Pd in Pd/SiO$_2$ is present as Pdδ+. This relatively strong interaction between Pd and defects on

SiO$_2$ explains the nucleation of Si on Pd/SiO$_2$ systems. For the non-activated system, Pd and Si nucleate separately and thus do not mix below the desorption temperature of Si. On the other hand, for the "activated" surface, the presence of Pdδ+ can preferentially lead to the adsorption of Si on or very near to the highly dispersed Pd followed by the formation of a silicic.

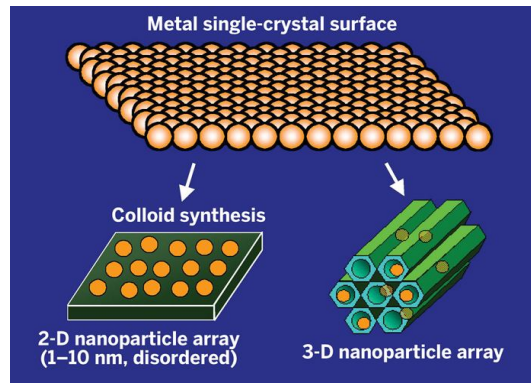### 1.9.3 Some Figures of Copper oxide Nano particles:
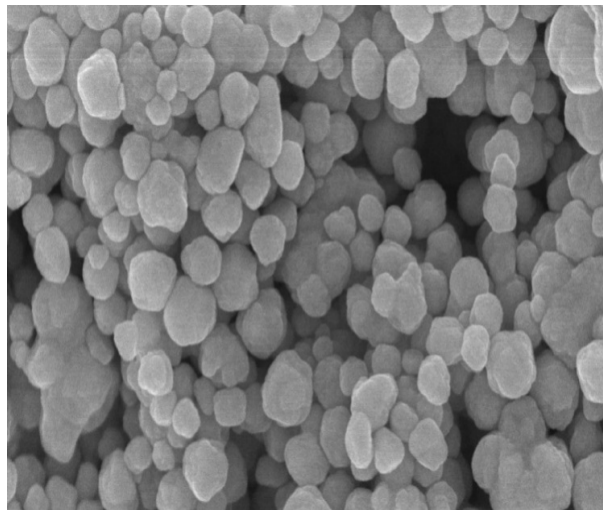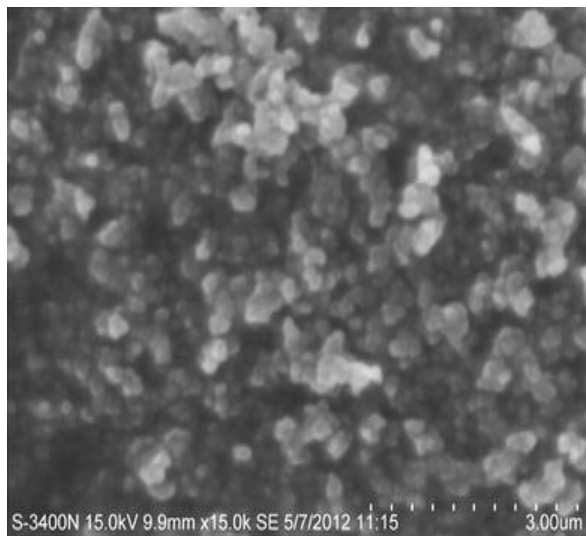

Figure 1.1 Metal single-crystal surface

Figure 1.2nanoparticles

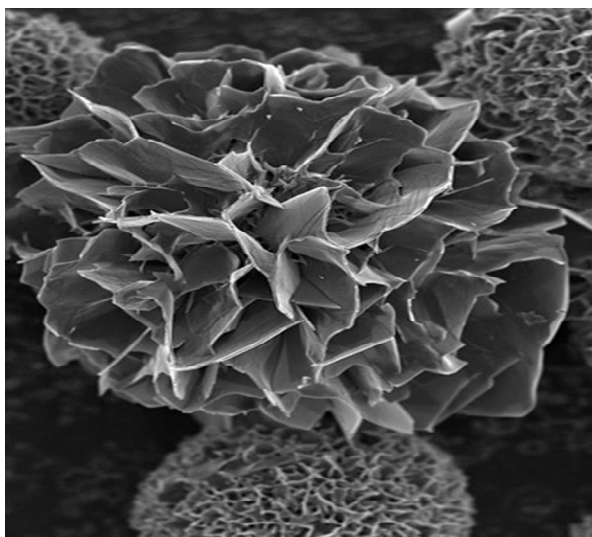**Figur1.3: crystal nanoparticle**

Figure 1.4: Semi nano particles

1.10 Objectives of the present study:

The objective of this present study can be divided to three parts which can be summarized as follows:

- Preparation of copper oxide by Sol -gel method.
- Preparation of catalyst copper oxide on silica.
- Characterization of the obtained products X-ray diffraction (XRD) spectroscopy and IR ,then comparison between copper oxide and supported copper oxide by silica.

Chapter two

Materials and Methods

2-Materials:

2.1Apparatuses and Equipments:

- Beakers (250ml) (Pyrex type).
- Hot plate Magnetic stirrer (SHIMADZU).
- Glass watch.
- X-ray diffraction (X-RD) spectroscopy (SHMADZU).
- Measuring cylinder.
- Whitman filter paper.
- Balance (SHIMADZU JAPAN).
- PH- meter (SHIMADZU JAPAN).
- Fourier transform-Infrared spectroscopy (FT-I spectroscopy) (SHIMADZU).

2.2 Chemicals:

All chemicals used in this research were of analytical grade type and it is includes:

- Sodium silicate (Na_2Si).
- Copper acetate Cu ($C_2H_3O_2$)$_2$.
- Glacial acetic acid ($CH_3.COOH$)
- Sodium hydroxide (NaOH).
- Silica (SiO_2).
- Distilled water.
- Sodium Thio salphate$Na_2S_2O_3$.

2.3 Preparation Methods:

2.3.1 Preparation of Ultra-Pure Silicon Dioxide:

30 g of sodium silicates were weighted and poured into a beaker (250ml), dissolved in 50 ml of hydrochloric acid, 50ml of water were added then shacked until the solution is completely dissolved, 35g of sodium bisulphate were dissolved in 100ml water, the solution was stirred vigorously with glass rode until its completely dissolved .the contents of the first beaker was poured into the second one and mixed thoroughly until a thick jelly-like precipitate was formed. The precipitate was poured into a porcelain crucible and heated. Dried and weighted the percentage of yield was calculated as following equation:

Yieid %= (Wprac/Wtheo) × 100.....

Where:

Wprac   practical weight

Wtheo   theoratical weigh

Wtheo   can be calculated from the theoretical number of moles of sodium silicates and sodium bisulphate.

2.4. Synthesis Method:

2.4.1 Preparation of CuO nanoparticles:

2.4.2 Sol-gel   Method of synthesis:

There are various techniques to prepare nanocrystals e.g. sputtering, laser ablation, cluster deposition, sol-gel method etc. In the present work the synthesis of CuO is preferred by sol-gel route because this method is easy and economical [24, 25]. The aqueous solution of Cu $(C_2H_3O)_{2.2H_2O}$ (0.2 M) is prepared in cleaned round bottom flask. 1 ml of glacial acetic acid was added to above aqueous solution and heated to 100 °C with constant stirring. 8 M NaOH was added to above heated solution till pH reaches to 7.

The color of the solution turned from green to black immediately and the large amount of black precipitate is formed immediately. The precipitate is centrifuged and washed 3 -4 times with deionized water. The obtained precipitate was dried in air for 24 hours. This powder is further used for the characterization of CuO nanoparticles.

2.5. Characterization Methods:

2.5.1. Percentage of Yield:

The percentage of Cu in copper oxide nanoparticles was done using titrimetric Methods.

2.5.2. X ray Diffraction (XRD):

X-ray diffraction (XRD) is a rapid analytical technique primarily used for phase identification of a crystalline material and can provide information on unit cell dimensions. The analyzed material is finely ground homogenized and average bulk composition is determined.

2.5.3. FT-IRspectroscopy:

IR spectroscopy was used to elucidate the structure and characteristic peak of copper oxide which was formed by the latter two method (2.3.1and2.4.1) and the spectra were recorded.

Chapter Three

3. Results and Discussion

3.1. Weight of Silicon Dioxide:

The obtained silicon dioxide has amorphous crystal structure white and the melting point was equal to 1650 C.

The obtained practical weight of silicon dioxide was 15.002g and the calculated percentage yield was 89.3% .The reaction equation for this preparation can be represented by the following equation:

$$Na_2SiO_3 + NHSO_4 \xrightarrow{ields} H_4SiO_3 \rightarrow (3.1)$$
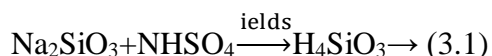
Silicon dioxide is stable in water and at high temperature. This chemical stability and good electrical insulation properties are the major reason that is needed to fabricate excellent semiconductor devices .The properties of silicon dioxide nano particles such as high surface areas are highly desirable as catalytic support because high surface area provides more active sites for gas or solid interaction .

From these points this method can be considerable good procedure to synthesis pure silicon dioxide.

3.2 X-ray diffraction (XRD):

The X-ray diffraction pattern of the CuO samples prepared in the presence of TG is depicted in Figure 2. It can be clearly seen that all the peaks in the XRD patterns are consistent with the JCPDS data (48-1548) of the CuO with a monoclinic phase. No characteristic peaks of any other impurities such as Cu $(OH)_2$, Cu_2O, or precursors used are formd.

3.3 Vibrational spectra:

Infrared spectra can be used to measure the M-O stanching frequency in metal aqua ions. Interpretation of the vibration frequencies is somewhat complicated by the presence, in octahedral and tetrahedral ions, of two vibrations, a symmetric one spectrum and an anti-symmetric one, measured in the infrared spectrum.

Although the relationship between vibration frequency and force constant is not simple, the general conclusion that can be taken from these data is that the strength of the M-O bond increases with increasing ionic charge and decreasing ionic size. The M-O stretching frequency of an aqua ion in solution may be compared with its counterpart in a crystal of known structure. If the frequencies are very similar it can be concluded that the coordination number of the metal ion is the same in solution as it is in a compound in the solid stat.

3.4 characterization of CuO nano particle and CuO supported on silica:

In the synthesis of CuO nanowires, when copper acetate reacted with sodium hydroxide in the aqueous medium, the reaction takes place as stated in Equation (3.2). This particular reaction does not involve any templates or substrates or any structure-directing agent like cetyltrimethylammonium-bromide [CTAB] or hex methylene tetra mine [HMTA] [82, 83]. However, we introduced the organic molecule TG to the copper acetate solution before reacting with NaOH. In the present synthesis, the concentration of Cu (OAc) $_2$ and NaOH and the reaction time are the critical parameters to obtain the nanowire morphology. Since the surface passivation of quantum dots using TG is well documented in literature [84, 85], we have tried to utilize for the very f+irst time the same organic molecule TG in the synthesis of CuO nanowires

$$CuCH_3 (COO)_2 \cdot H2O + NaOH \rightarrow TGCuO + 2Na (CH_3COO) + H_2O \quad (3.2)$$

When the reaction in Equation 3.2 proceeds with the nucleation and crystal growth, the Gibbs free energy of the nanocrystallites surfaces is very high, and in order to decrease the Gibbs free energy, the nanocrystallites tend to aggregate [86]. The flower morphology of CuO is obtained. When a small amount of TG is introduced in the synthesis of CuO, instead of a flower morphology, well-dispersed CuO nanowires are obtained, which can be speculated due to the stabilization effect caused by the use of organic molecule TG. Moreover, the role of TG is different from what structure-directing agents such as CTAB and HMTA are doing. In our case, without any structure-directing agent, we are able to generate CuO Nano flowers.

In order to detect the elements present in the CuO samples

Only separated CuO nanowires which clearly imply that the role of TG is definitely observed, indicating the formation of a pure phase CuO.

Depend on the result which mentioned above different band between copper oxide nano particles and copper oxide supported on silica due to the band of CuO paper clearly on 37,42,51and 65,this results indicated copper oxide crystal, another hand copper oxide supported on silica make suppress on the main ship due to presence of silica and became amphora's.
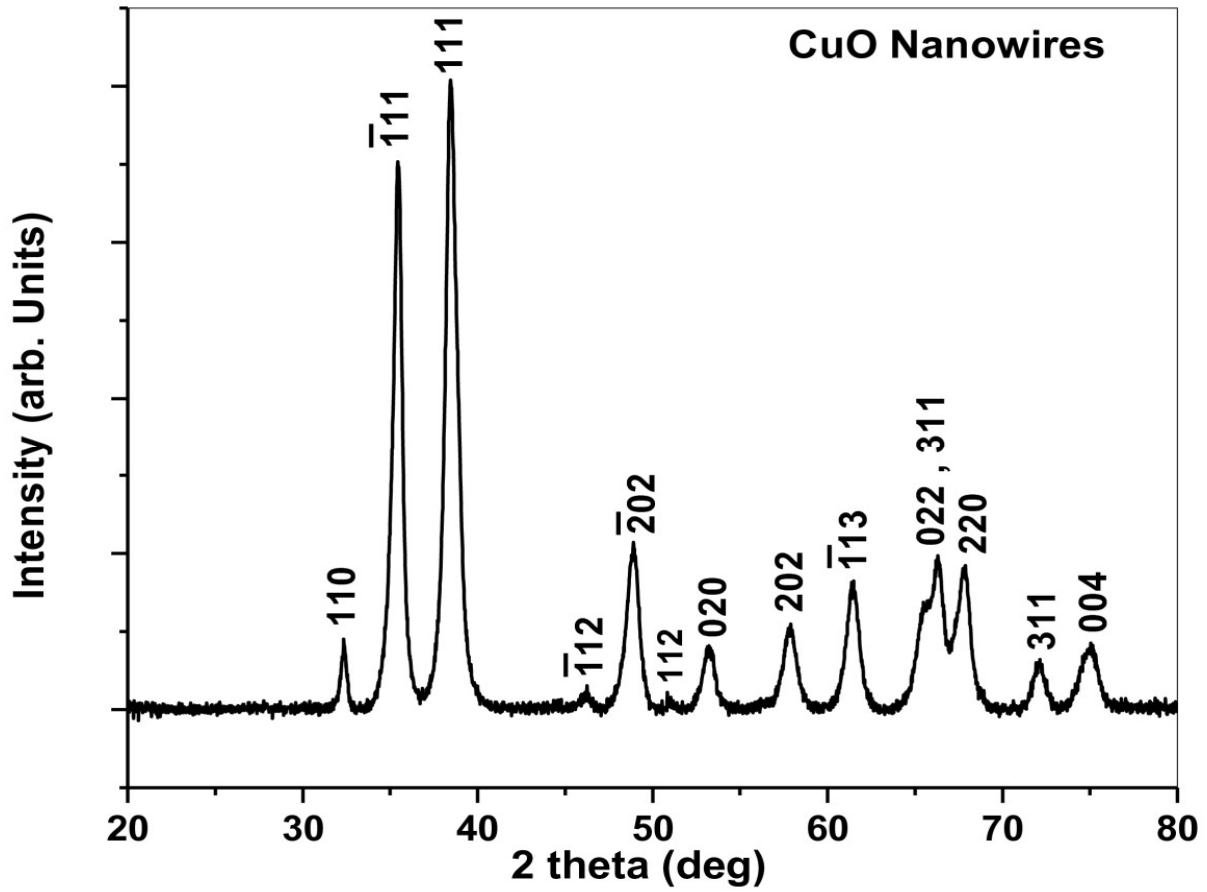
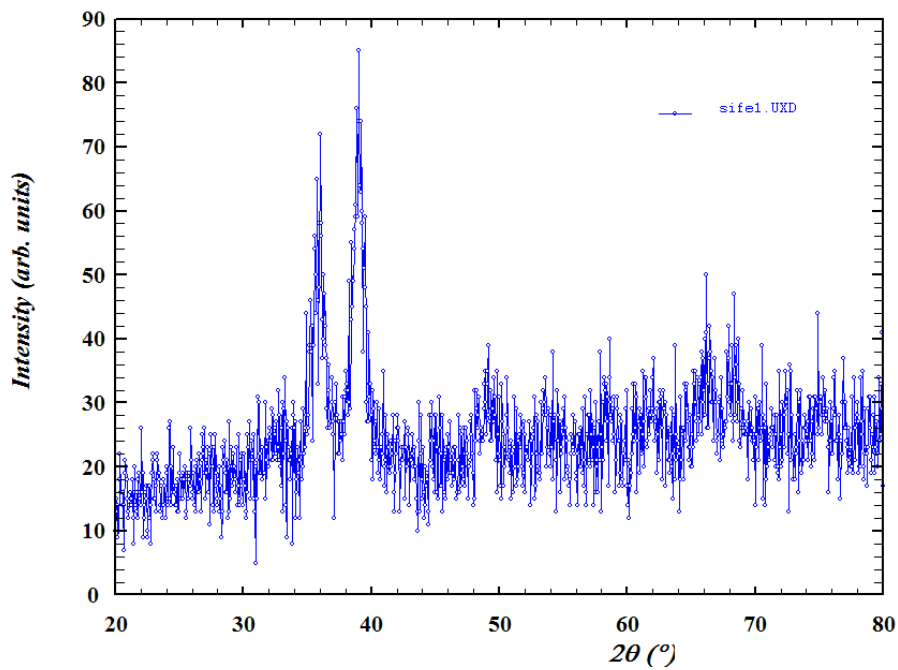**Figure 3.1 XRD pattern of the as-synthesized CuO nanowires with TG.**

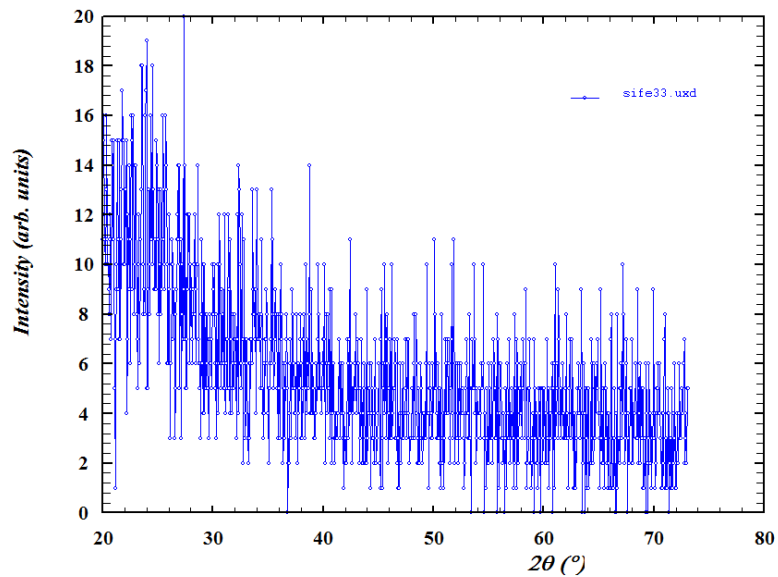**Figure 3.2 XRD of copper oxide nano particale**

Figure 3.3 XRD of copper oxide nano particale Supported on silica

In order to understand the chemical an0d structural nature of the synthesized CuO and the effect of the chemicals used in the synthesis of CuO nanowires, FTIR analysis was carried out. Figure 3 represents the FTIR spectrum recorded for the CuO nanowires in the range of 400 to 4,000 cm^{-1}. The three characteristic bands observed at 432.3 cm^{-1}, 497 cm^{-1}, and 603.3 cm^{-1} can be assigned to the Au mode, Bu mode, and the other Bu mode of CuO [87]. The high-frequency mode at 603.3 cm^{-1} may be attributed to the Cu-O stretching, while the peak at 497 cm^{-1} can be assigned to the Cu-O stretching vibration along [88]. Moreover, no other IR active mode was observed in the range of 605 to 660 cm^{-1}, which totally rules out the existence of another phase, i.e., Cu_2O [89]. Moreover, the C-S bond observed at 661.4 cm^{-1} can be attributed to the organic molecule TG used in the synthesis of CuO nanowires. Thus, the pure phase CuO with monoclinic structure is also confirmed from the FTIR analysis.
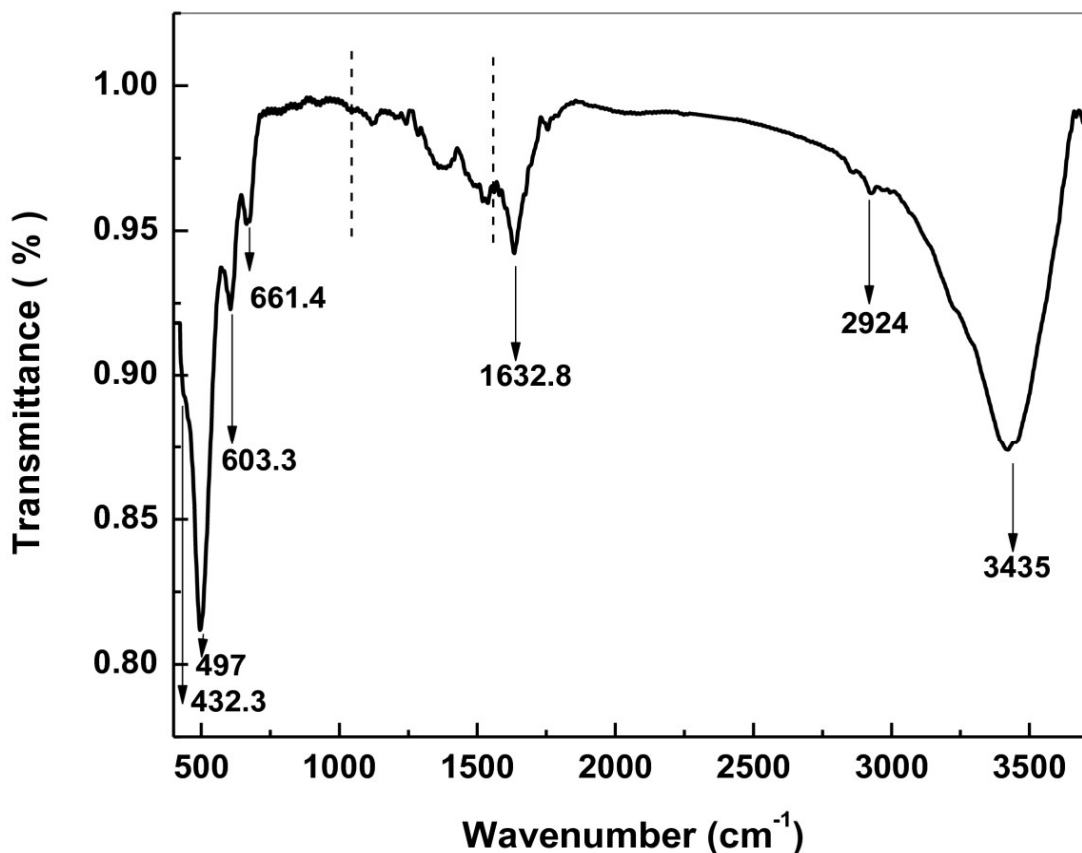

Figure 3.4 IR of copper oxide supported on silica

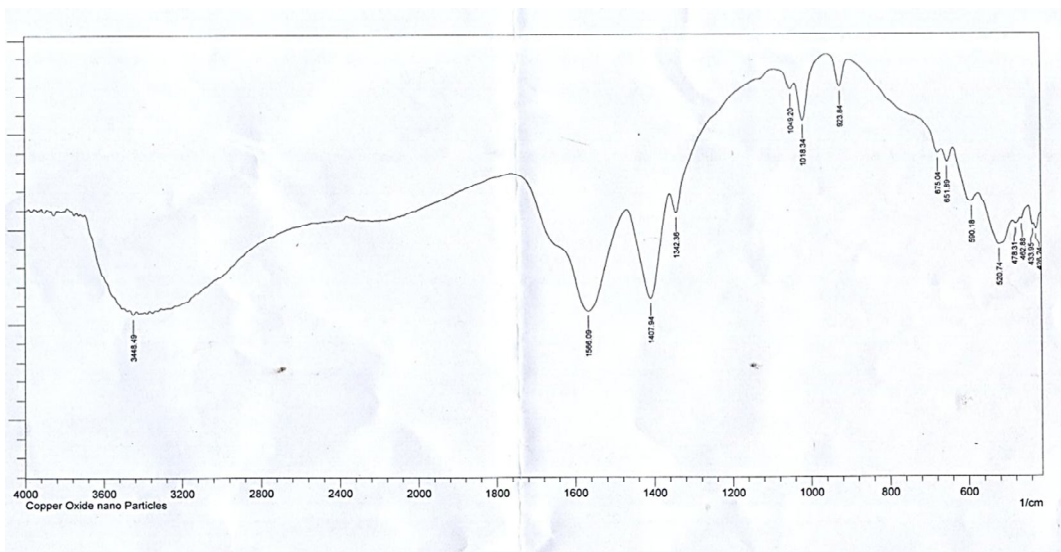The FTIR spectrum of the as-synthesized CuO nanowires in the presence of TG.

Figure 3.5 IR of copper oxide nano particle

From figure 3.5:The band 3448.49cm assigned to the OH ,651.89cm C-S bond ,590.18,520.74,478.31,462.8 and,433.95,can be assigned to the CuO.

The high frequency at 651.89and675.01cm may be attributed to the Cu-O can be assigned to the Cu-O stretching vibration.

4. Conclusions:

Using a simple and inexpensive wet chemical method, the synthesis of copper oxide nanowires has been successfully carried out. The concentration and quantity of precursors are the critical factors for obtaining the desired 1-D morphology due to the stabilization effect of the surface, on the other hand the shape of copper oxide supported on silica obtain different due to the suppressor of band .The FTIR data analyses confirm the formation of a pure phase CuO with monoclinic crystal structure and morphology structure for copper oxide nano particle supported on silica. XRD data support the same finding.

5. Recommendations:

Obtain better results, recommend to use more modern apparatus such as (LEED), (SEM), (STM) AND (XPS) and usage of more process in different applications.

References:

1. Module 3: Characteristics of Particles – Particle Size Categories. epa.gov

2. Taylor, Robert; Coulombs, Sylvain, Otanicar, Todd; Phelan, Patrick, Gunawan, Andrey, Lv, (2013), (Small particles, big impacts: A review of the diverse applications of Nano fluids), *Journal of Applied Physics* **113**

3. Taylor, Robert, A, Otanicar, Todd; Rosengarten, Gary, (2012), (Nanofluid-based optical filter optimization for PV/T systems), *Light*

4. Science & Applications 1 (10): e34.

5. Hewakuruppu, Y. L, Dombrovsky, L. A, Chen, C, Timchenko, V, Jiang, X, Baek, S, Taylor, R. A, (2013), (Plasmonic "pump–probe" method to study semi-transparent nanofluids), *Applied Optics*, **24**, 6041–6050.

6. Taylor, Robert, A, Otanicar, Todd P, Herukerrupu, Yasitha, Bremond, Fabienne, Rosengarten, Gary, Hawkes, Evatt R, Jiang, Xuchuan, Coulombe, Sylvain, (2013).

7. Bibcode ,(2013),(Feasibility of nanofluid-based optical filters), *Applied Optics*,**52.**

8. Khan, Firdos, Alam, (2012), (Biotechnology Fundamentals), *CRC Press*.

9. Faraday, Michael, (1857), (Experimental relations of gold (and other metals) to light*). Phil. Trans. Roy. Soc. London*, **147**, 145–181.

10. Beilby, G.T, (1903), (The Effects of Heat and of Solvents on Thin Films of Metal), *Proceedings of the Royal Society*, **72**, 477–486.

11. Turner, T, (1908), (Transparent Silver and Other Metallic Films), *Proceedings of the Royal Society*, **548**, 301–310.

12. Buffat, Ph, Borel, J.P, (1976), (Size effect on the melting temperature of gold particles), *Physical Review*, **6**, 2287–2298.

13. Taylor, Robert A,Phelan, Patrick E, Otanicar, Todd P, Adrian, Ronald, Prasher, (2011), (Nanofluid optical property characterization: Towards efficient direct absorption solar collectors),*Nanoscale Research Letters* , **1**, 225.

14. Gubin, Sergey P, (2009), (Magnetic nanoparticles), *Sunscreen.U.S. Food and Drug Administration.*

15. Mitchnick, MA, Fairhurst, D, Pinnell, SR, (1999), (Microfine zinc oxide (Z-cote) as a photostable UVA/UVB sunblock agent), *Journal of the American Academy of Dermatology*, **1**, 85–90.

16. Heim, J, Felder, E, Tahir, MN; Kaltbeitzel, A, Heinrich, UR, Brochhausen, C, Mailänder, (2015), (Genotoxic effects of zinc oxide nanoparticles.), *Nanoscale*, **19**.

17. Wang, B, Zhang, Y, Mao, Z; Yu, D, GAO, C, (2014), (Toxicity of ZnO nanoparticles to macrophages due to cell uptake and intracellular release of zinc ions), *Journal of Nanoscience and Nanotechnology, 8*.

18. Gosens, I, Kermanizadeh, A, Jacobsen, NR, Lenz, AG, Bokkers, B; de Jong, WH; Krystek, P, Tran, L,Stone, V; Wallin, H; Stoeger, T, Cassee, FR, (2015), (Comparative hazard identification by a single dose lung exposure of zinc oxide and silver nanomaterials in mice), *PLOS ONE*, **5**.

19. Hanagata, N, Morita, H, (2015), (Calcium ions rescue human lung epithelial cells from the toxicity of zinc oxide nanoparticles), *The Journal of toxicological sciences*, **5**, 625–35.

20. Kim, YH, Kwak, KA, Kim, TS, Seok, JH, Roh, HS, Lee, JK, Jeong, J, Meang, EH, Hong, JS; Lee, YS, Kang, JS, (2015), (Retinopathy Induced by Zinc Oxide Nanoparticles in Rats Assessed by Micro-computed Tomography and Histopathology),*Toxicological research* , **2**, 157–63.

21. Moridian, M, Khorsandi, L, Talebi, AR (2015), (Morphometric and stereological assessment of the effects of zinc oxide nanoparticles on the mouse testicular tissue),*Bratislavske lekarske listy,* **116**, (5), 321–5.

22. Chon C.H., K.D.Kihm, (Thermal Conductivity Enhancement of Nanofluid by Browian Motion) *ASME Journal Heat Transfer* **12**, (2005), pp 810.

23. Das S.K, Putra N,Thiesen P, Roetzel w, (Temperature Dependence of thermal conductivity enhancement for nanofluids), *ASME Journal Heat Transfer,* **125,**(2003), PP 567.

24. M, Nagaraju, K, Mukkanti, R, BuchiReddy, Y, Aparna, NCONSEA (National Conference on Nano science and nano engineering application), **op025**, 31(2012).

25. Y.Aparna, K.Venkateswara Rao, P, Srinivasa Subbarao, (Preparation and Characterization of CuO Nanoparticles by Novel Sol-Gel Technique), *Journal of Nano and Electronic Physics 4, (2012)*, **pp 3005**, (1-4).

26. S.A. Stevenson, R.T.K. Baker, J.A. Dumesic, E, Ruckenstein (Eds.), (Metal–Support Interactions in Catalysis, Sintering, and Redispersion, Catalysis Series, Van Nostrand Reinhold), *New York*, 1987.

27. M. Valden, X. Lai, D.W. Goodman**, Science 281**, (1998), 5383.

28. M. Haruta, Catal, Today **36**, (1997), 153.

29. S.J. Tauster, S.C. Fung, R.L. Garten, J. Am. Chem. Soc. **100**, (1978), 170.

30. S.J. Tauster, S.C. Fung, R.T.K. Baker, J.A. Horsley, **Science 221**, (1981), 1121.

31. Katrib, C. Petit, P. Legare, L. Hilaire, G. Maire, Surf**. Sci. 189–190**, (1987), 886.

32. R. Lamber, N. Jaeger, G. Schulz-Ekloff, Surf. **Sci. 227**, (1990), 268.

33. R. Lamber, W. Romanowski, J. Catal, **105**, (1987), 213.

34. T.-C. Chang, J.-J. Chen, C.-T. Yeh, J. Catal, **96**, (1985), 51.

35. R. Pretorius, J.M. Harris, M.-A. Nicolet, (Solid-State Electron), **21**, (1978), 667.

36. M. Chen, L.D. Schmidt, J. Catal, **55**, (1978), 348.

37. X. Xu, J.-W. He, D.W. Goodman, Surf, *Sci. 284*, (1993), 103.

38. X. Xu, D.W. Goodman, Appl. Phy, Lett, **61**, (1992), 1799.

39. X. Xu, J. Szanyi, Q. Xu, D.W. Goodman, Catal, Today **21**, (1994), 57.

40. B.R. Powell, S.E. Whittington, J. Catal, **81**, (1983), 382.

41. L.C.A. Van den Oetelaar, A. Partridge, S.L.G. Toussaint, C.F.J. Flipse, H.H.Brongersma, *J. Phy, Chem,* B **102**, (1998), 9541.

42. D.W. Scott, S.S. Lau, Thin Solid Films, **104**, (1983), 227.

43. B. Schleich, D. Schmeisser, W. Gopel, Surf, **Sci. 191**, (1987), 367.

44. R. Anton, U. Neukirch, M. Harsdorff, Phys, Rev B **36**, (1987), 7422.

45. R. Anton, (Thin Solid Films), **118**, (1984), 293.

46. J.T. Mayer, R.F. Lin, E. Garfunkel, Surf, **Sci. 265**, (1992), 102.

47. J.B. Zhou, T. Gustafsson, R.F. Lin, E. Garfunkel, Surf, **Sci. 284,** (1993), 67.

48. S.M. Goodnick, M. Fathipour, D.L. Ellsworth, C.W. Wilmsen, J. Vac. Sci. Technol, **18,** (1981), 949.

49. R. Lamber, (Thin Solid Films), **128,** (1985), L29.

50. H. Praliaud, G.A. Martin, J. Catal, **72**, (1981), 394.

51. H. Dallaporta, M. Liehr, J.E. Lewis, Phys. Rev, B **41,** (1990), 5075.

52. M. Liehr, H. Dallaporta, J.E. Lewis, Appl, Phys. Lett, **53**, (1988), 589.

53. L.C.A. Van den Oetelaar, R.J.A. Van den Oetelaar, A. Partridge, C.F.J. Flipse, H.H.Brongersma, Appl. Phys, Lett, **74**, (1999), 2954.

54. B.K. Min, A.K. Santra, D.W. Goodman, J. Vac, Sci, *Technol, in press.*

55. S.M. Sze, (VLSI Technology, McGraw-Hill), *New York,* 1983.

56. M. Liehr, H. Lefakis, F.K. Legoues, G.W. Rubloff, Phys, Rev, B **33**, (1986) ,5517.

57. L.-L. Shen, Z. Karpinksi, W.M.H. Sachtler, J. Phys, Chem, **93**, (1989), 4890.

58. W. Juszczyk, Z. Karpinski, J. Catal, **117**, (1989), 519.124 B.K. Min et al. / Catalysis Today, **85**, (2003), 113–124.

59. X. Lai, T.P. St. Clair, M. Valden, D.W, Goodman, Prog, Surf. Sci, **59**, (1998), 25.

60. R.L. Moss, D. Pope, B.J. Davis, D.H. Edwards, J. Catal, **58**, (1979), 206.

61. G.A. Martin, J.A. Dalmon, J. Catal, **75**, (1982), 233.

62. G.A. Martin, J.A. Dalman, (React. Kinet. Catal), Lett, **16**, (1981), 325.

63. G.A. Martin, R. Dutartre, J.A. Dalman, (React. Kinet. Catal), Lett. 16 (1981) 329.

64. M. Primet, J.A. Dalmon, G.A. Martin, J. Catal, **46**, (1977), 25.

65. P. Wynblatt, N.A. Gorstein, (Acta Metall), **24**, (1976), 1165.

66. C.H. Bartholomew, Appl. Catal, A, **107**, (1993), 1.

67. H. Poppa, (Thin Solid Films), **34**, (1976), 94.

68. J.J. Chen, E. Ruckenstein, J. Catal, **69**, (1981), 254.

69. X. Xu, D.W. Goodman, J. Phys. Chem. 97 (1993) 683.

70. X. Xu, S.M. Vesecky, D.W. Goodman, Science **258**, (1992), 788.

71. X. Xu, S.M. Vesecky, J.-W. He, D.W. Goodman, J. Vac. Sci. Technol, A, **11**, (1993), 1930.

72. A.K. Santra, B.K. Min, D.W. Goodman, Surf. Sc, **515**, (2002), L475.

73. A.K. Santra, B.K. Min, D.W. Goodman, Surf. Sc, **513**, (2002), L441.

74. E. Ozensoy, B.K. Min, D.W. Goodman, J. Phys. Chem. B, (submitted for publication).

75. Y.D. Kim, T. Wei, D.W. Goodman, Langmuir, **19**, (2003), 354.

76. A. Bogicevic, D.R. Jennison, Surf. Sci, **515**, (2002), L481.

77. B. Carriere, B. Lang, Surf. Sci, **64**, (1977), 209.

78. E. Kampshoff, N. Walchli, K. Kern, Surf, Sci, **406**, (1998), 117.

79. N. Walchli, E. Kampshoff, A. Menck, K. Kern, Sur, Sci, **382**, (1997), L705.

80. V. Lyubinetsky, V.K. Adamchuk,(Thin Solid Films), **288**, (1996), 182.

81. K. Tanaka, K. Furui, M. Yamada, J. Phys, So, Jpn, **64**, (1995).